Published in final edited form as:
*Biomaterials*. 2011 December ; 32(34): 8990–8998. doi:10.1016/j.biomaterials.2011.08.035.

# The development of collagen-GAG scaffold-membrane composites for tendon tissue engineering

**Steven R. Caliari**[a], **Manuel A. Ramirez**[b], and **Brendan A.C. Harley**[a,c,*]

[a]Dept. Chemical and Biomolecular Engineering, University of Illinois at Urbana-Champaign, Urbana, IL 61801, USA

[b]Dept. Bioengineering, University of Illinois at Urbana-Champaign, Urbana, IL 61801, USA

[c]Institute for Genomic Biology, University of Illinois at Urbana-Champaign, Urbana, IL 61801, USA

## Abstract

Current tissue engineering approaches for tendon defects require improved biomaterials to balance microstructural and mechanical design criteria. Collagen-glycosaminoglycan (CG) scaffolds have shown considerable success as *in vivo* regenerative templates and *in vitro* constructs to study cell behavior. While these scaffolds possess many advantageous qualities, their mechanical properties are typically orders of magnitude lower than orthopedic tissues such as tendon. Taking inspiration from mechanically efficient core–shell composites in nature such as plant stems and porcupine quills, we have created core–shell CG composites that display high bioactivity and improved mechanical integrity. These composites feature integration of a low density, anisotropic CG scaffold core with a high density, CG membrane shell. CG membranes were fabricated via an evaporative process that allowed separate tuning of membrane thickness and elastic moduli and were found to be isotropic in-plane. The membranes were then integrated with an anisotropic CG scaffold core via freeze-drying and subsequent crosslinking. Increasing the relative thickness of the CG membrane shell was shown to increase composite tensile elastic modulus by as much as a factor of 36 in a manner consistent with predictions from layered composites theory. CG scaffold-membrane composites were found to support tendon cell viability, proliferation, and metabolic activity *in vitro*, suggesting they maintain sufficient permeability while demonstrating improved mechanical strength. This work suggests an effective, biomimetic approach for balancing strength and bioactivity requirements of porous scaffolds for tissue engineering.

### Keywords

Collagen; Scaffold; Membrane; Composite; Tendon; Mechanical properties

## 1. Introduction

Tendons are specialized connective tissues that transmit tensile loads between bone and muscle. Their functional capacity derives from a unique extracellular matrix (ECM) composed primarily of type I collagen arranged in a highly organized hierarchy of parallel, crosslinked fibrils [1,2]. Tendon and ligament injuries are common among both recreational



*Corresponding author. Dept. of Chemical and Biomolecular Engineering, Institute of Genomic Biology, University of Illinois at Urbana-Champaign, 110 Roger Adams Laboratory, 600 S. Mathews Ave., Urbana, IL 61801, USA. Tel.: +217 244 7112; fax: +217 333 5052. bharley@illinois.edu. .

and elite athletes as well as the elderly. Of the near 35 million musculoskeletal injuries in the US every year, approximately 50% involve tendons and ligaments with a cost to the US health care industry in the tens of billions of dollars per year [3]. The most serious injuries require surgical intervention; such tendon and ligament injuries are responsible for hundreds of thousands of surgical procedures each year in the US [2,3].

One of the key challenges of orthopedic tissue engineering is to create biomaterials that can support tissue regeneration while remaining mechanically competent. Due to the need for mechanical competence, the most common biomaterial designs for tendon and ligament tissue engineering are electrospun polymer mats [4–6] and woven fibrous materials [7,8]. While these constructs can promote cell alignment and be designed with tensile moduli approaching the level of tendon, they are dense substrates that permit limited cell penetration compared to the traditional tissue engineering target for a fully three-dimensional biomaterial structure. As an alternative, porous scaffold biomaterials typically have highly tunable 3D microstructural features, show significantly heightened levels of permeability, and can be fabricated from a range of natural, biodegradable materials. However, the relative density ($\rho^*/\rho_s$; 1% porosity where $\rho^*$ is the density of the porous foam and $\rho_s$ is the density of the solid it is constructed from) of these porous scaffolds differentially affects a number of critical scaffold properties. Notably, increasing scaffold $\rho^*/\rho_s$ increases both its specific surface area, impacting cell attachment, and its elastic modulus, which varies with $(\rho^*/\rho_s)^2$ [9–12]. However, increasing scaffold $\rho^*/\rho_s$ also increases steric hindrance to cell penetration and, critically, reduces scaffold permeability [13], negatively impacting cell penetration into the porous structure and long-term survival. Due to the high porosity (>90%) typically required for most tissue engineering scaffolds to adequately support cell bioactivity [14], these materials are often orders of magnitude too soft for orthopedic applications such as for tendon. Mechanical stimulation of cell-seeded scaffold constructs has been used to marginally improve construct mechanical properties, however not to the level of native tendon or ligament [15–18]. Coupled with the known anisotropy of native tendon tissue, strategies to produce mechanically-reinforced, anisotropic biomaterial scaffolds may present a pathway toward developing bioactive tendon regeneration templates.

Porous collagen-glycosaminoglycan (CG) scaffolds have previously been used in a variety of tissue engineering applications, both *in vivo* as regenerative templates for skin, peripheral nerves, conjunctiva, and cartilage [19–21] as well as *in vitro* as 3D micro-environments to probe fundamental questions about cell behaviors and cell–matrix interactions [22–26]. These scaffolds have pore microstructures designed to simultaneously block cell-mediated contraction and scar tissue synthesis while supporting cell attachment, proliferation, efficient metabolite transport, and synthesis of a functional ECM [11,21]. Notably, their chemical composition and degradation kinetics have been specifically optimized to prevent platelet accumulation and organized wound contraction [21]. The CG scaffolds are traditionally fabricated via freeze-drying where the freezing rate [27] and final freezing temperature [22,28] can be manipulated to affect scaffold pore size and uniformity. Recently, a directional solidification approach has been introduced that enables fabrication of a series of highly anisotropic CG scaffolds characterized by aligned tracks of ellipsoidal pores for tendon tissue engineering applications [29]. A significant effect was observed for both pore shape (anisotropic vs. isotropic) and anisotropic scaffold pore size (50–250 μm) on the attachment, proliferation and metabolic activity of primary equine tendon cells [29]. These CG scaffolds possess the 3D structure, porosity (>95%), and bioactivity required of an orthopedic regeneration template, but mechanically are 2–3 orders of magnitude softer than native tendon ($E^* \sim 10^2$–$10^3$ MPa) [30,31]. Alternatively, a series of collagen membranes have recently been described for applications in skin [32], peripheral nerve [33], and bone [34] repair. These membranes provide an avenue to theoretically present the same

combinations of bioactive ligands as CG scaffolds but with improved mechanical properties. However, these collagen membranes lack a 3D microstructure or the porosity required for cell integration.

While the multi-scale properties of tendon itself cannot be replicated by current biomaterials technologies, composite materials that mimic mechanically efficient core–shell structures in nature may hold promise for complex tissue engineering applications. Plant stems combine a porous core with a dense shell to aid osmotic transport (core) while maintaining sufficient tensile/bending stiffness (shell); bird beaks and porcupine quills can also combine a dense shell and porous core to enhance compressive strength and mechanical efficiency, respectively [10]. Core-shell composite designs have been used to engineer high strength structural materials [35], but have not seen extended application in the field of biomaterials. A composite biomaterial that combines, but does not functionally integrate, an agarose hydrogel and a nanofiber electrospun mat has recently been described for fibrous tissue (intervertebral disk, meniscus) regeneration applications [36]. A recently described liquid-phase co-synthesis methodology provides the ability to create composite CG scaffolds featuring multiple, distinct biomaterial compartments linked together by a continuous interface [37]. While originally developed to link two disparate scaffold compartments for osteochondral tissue engineering, this technology provides a pathway for creating a novel composite biomaterial that functionally integrates CG scaffold and membrane elements. We believe adding the CG membrane can significantly increase the tensile strength of the subsequent scaffold-membrane composite in a manner consistent with layered composite theory predictions [38].

This manuscript describes the development of a new class of core–shell CG biomaterial composites that integrate a high density (high tensile strength) isotropic CG membrane with a low density (highly porous) anisotropic CG scaffold (Fig. 1). We hypothesized that the CG membranes could be integrated with aligned CG scaffolds in a manner to maintain adequate permeability to support tendon cell proliferation and bioactivity. Such a composite biomaterial is hypothesized to improve regenerative capacity by significantly improving construct mechanical integrity while still presenting a highly porous scaffold microstructure containing aligned contact guidance cues. To our knowledge, biomaterial composites that integrate scaffold and membrane components to mimic core–shell designs found in nature have not previously been described, but potentially offer significant value for musculoskeletal tissue engineering.

## 2. Materials and methods

### 2.1. CG suspension preparation

CG suspensions were prepared from type I microfibrillar collagen (0.5% w/v) isolated from bovine dermis (Devro Inc., Columbia, SC) and chondroitin sulfate (0.05% w/v) derived from shark cartilage (Sigma–Aldrich, St. Louis, MO) in 0.05 M acetic acid [19]. The suspension was homogenized at 4 °C to prevent collagen gelatinization during mixing and was subsequently degassed before use.

### 2.2. CG membrane fabrication

CG membranes were fabricated from the CG suspension via an evaporative process modified from previously described methods [39]. Briefly, the degassed CG suspension was pipetted into a Petri dish and allowed to air dry in a chemical fume hood at room temperature for 2–3 days. In order to create a series of CG membranes of variable thickness, a series of membranes were fabricated via the identical method but using CG suspension of different volumes (25–50 mL) and/or densities (0.5% w/v, 1% w/v). The primary membrane

variants tested were 0.5% w/v 25 mL, 0.5% w/v 50 mL, 1% w/v 25 mL, and 1% w/v 50 mL. Another membrane was fabricated by sequential addition of 1% w/v CG suspension to the same Petri dish (150 mL total volume).

### 2.3. Aligned CG scaffold and composite fabrication

Aligned CG scaffolds ($\rho^*/\rho_s$ = 0.006) were fabricated as previously described [29]. Briefly, the CG suspension was added to wells of a multicomponent polytetra-fluoroethylene (PTFE)-copper mold, and placed on a freeze-dryer shelf (VirTis Genesis, Gardiner, NY) at a pre-cooled temperature (−10 °C or −60 °C) in order to promote directional solidification. After freezing, ice crystals were sublimated under vacuum (200 mTorr) at 0 °C to produce CG scaffolds (6 or 8 mm diameter, 15 or 30 mm length) displaying aligned pores (−10 °C: 243 ± 29 μm; −60 °C: 55 ± 18 mm) [29]. Mechanical tests were performed on 6 mm diameter by 30 mm length scaffolds to facilitate placement of the constructs within the mechanical tester grips.

Scaffold-membrane constructs were fabricated by first cutting CG membrane pieces to size and placing circumferentially within the PTFE-copper mold. The CG suspension was then pipetted inside the rolled membrane and allowed to hydrate the membrane for ~15 min at 4 °C before the mold was placed into the freeze-dryer held at a final freezing temperature of −10 °C; freezing and sublimation steps for these scaffold-membrane constructs were performed exactly as with the anisotropic scaffolds alone. Membrane hydration and subsequent freeze-drying was hypothesized to promote the integration of the scaffold structure with the membrane [37].

### 2.4. SEM analysis

Qualitative analysis of scaffold, membrane, and scaffold-membrane composite microstructure was performed using scanning electron microscopy (SEM). SEM analysis was performed with a JEOL JSM-6060LV Low Vacuum Scanning Electron Microscope (JEOL USA, Peabody, MA) using both a standard secondary electron (SE) detector and a backscatter electron (BSE) detector under low vacuum mode, bypassing the need for any sample sputter coating steps [37].

### 2.5. Crosslinking

Scaffolds, membranes, and scaffold-membrane composites were sterilized and dehydrothermally (DHT) crosslinked at 105 °C for 24 h under vacuum (<25 torr) in a vacuum oven (Welch Vacuum Technology, Niles, IL) prior to use [12,19]. Scaffolds and composites were then immersed in 100% ethanol overnight, washed with phosphate-buffered saline (PBS) several times over 24 h, and then crosslinked using carbodiimide chemistry [12,40] for 1 h in a solution of 1-ethyl-3-[3-dimethylaminopropyl]carbodiimide hydrochloride (EDAC) and *N*-hydroxysulfosuccinimide (NHS) at a molar ratio of 5:2:1 EDAC:NHS:COOH. To test the effect of crosslinking density on membrane mechanics, some membranes were hydrated directly in PBS without further crosslinking (Non-crosslinked, NC) or were crosslinked using EDAC chemistry at a molar ratio of either 1:1:5 or 5:2:1 EDAC:NHS:COOH. Scaffolds, membranes, and composites were subsequently stored in PBS until use.

### 2.6. Determination of membrane microstructural properties

Membrane thickness was determined from cross-sectional SEM images. Six 500× magnification images were taken for each membrane type, and the thickness of the membrane was measured using a multipoint measuring tool within the SEM software. The relative density ($\rho^*/\rho_s$) of each CG membrane type was determined from the calculated

density of the membrane ($\rho^*$) relative to the known density of solid collagen ($\rho_s$, 1.3 g cm$^{-3}$) [12,41,42]. Swelling kinetics and final swelling ratio of each CG membrane variant was determined by monitoring the weight of 2 cm by 2 cm membranes samples ($n$ = 6) hydrated in PBS for 5, 10, 15, 30 and increasing 30 min intervals up to 240 min. A normalized swelling curve was calculated for each membrane variant and the time required for complete hydration was defined as the point where the curve reached a plateau [43].

### 2.7. Mechanical characterization

Tensile tests were performed to on CG membranes (12 mm width, 45 mm length), aligned scaffolds (6 mm diameter, 30 mm length), and core–shell scaffold-membrane composites (6 mm diameter, 30 mm length). Choice of sample geometry was dictated by the size of the scaffolds and scaffold-membrane composites that will be deployed in subsequent *in vivo* regeneration studies. Tensile tests were performed in a manner consistent with previous mechanical analysis of CG scaffolds [12,44]. Specimens were hydrated in PBS for 24 h prior to testing and were then pulled to failure at a rate of 1 mm/min using an MTS Instron 2 (Eden Prairie, MN) with rubberized grips to prevent slip. Tensile modulus was calculated from the slope of the stress-strain curve over a strain range of 5–10% in the case of scaffolds and composites [9] and over the initial linear region for membranes [44]. For comparison to the anisotropic scaffolds, previously reported mechanical data for an isotropic control CG scaffold with a consistent relative density was used [45]. All samples tested were hydrated in PBS unless otherwise specified. Layered composites theory was applied to predict the tensile modulus ($E^*_{\text{composite}}$) of the final composites from the relative size and modulus of scaffold (composite radius, $r$; ($E^*_{\text{scaffold}}$) and membrane (membrane thickness, $t$; ($E^*_{\text{membrane}}$)) components and their separate moduli [38]:

$$E^*_{\text{composite}} = E^*_{\text{scaffold}} \left( \frac{(r-t)^2}{r^2} \right) + E^*_{\text{membrane}} \left( 1 - \frac{(r-t)^2}{r^2} \right) \quad (1)$$

### 2.8. Tendon cell culture and bioassays

**2.8.1. Tendon cell isolation and expansion—**Tendon cells (TCs) were isolated from horses aged 2–3 years euthanized for reasons not related to tendinopathy using previously described methods [46]. TCs were then expanded in standard culture flasks in high glucose Dulbecco's modified Eagle's medium (DMEM, Fisher Scientific, Pittsburgh, PA) supplemented with 10% fetal bovine serum (FBS, Invitrogen, Carlsbad, CA), 1% L-glutamine (Invitrogen, Carlsbad, CA), 1% penicillin/streptomycin (Invitrogen, Carlsbad, CA), 1% amphotericin-B (MP Biomedical, Solon, OH), and 25 μg/mL ascorbic acid (Wako, Richmond, VA) [46]. TCs were fed every 3 days and cultured to confluence at 37 °C and 5% $CO_2$. After expansion TCs were either frozen (50% DMEM, 40% FBS, 10% DMSO in liquid nitrogen) for later experiments or used (passage 3) for scaffold culture.

**2.8.2. CG scaffold tendon cell seeding and culture—**CG scaffold pieces (8 mm diameter, ~5 mm thickness, with and without outer membrane) were cut from the middle section of 8 mm diameter by 15 mm length scaffolds and placed in ultra-low attachment 6 well plates (Corning Life Sciences, Lowell, MA). Confluent TCs were trypsinized and resuspended at a concentration of $5 \times 10^5$ cells per 20 μL media. Scaffolds were initially seeded with 10 μL of cell suspension, incubated at 37 °C for 15 min, turned over, and seeded with an additional 10 μL of cell suspension for a total of $5 \times 10^5$ cells per scaffold as previously described [29]. Scaffolds were incubated at 37 °C and 5% $CO_2$ for the duration of all experiments and were fed with complete DMEM that was changed every 3 days.

**2.8.3. Quantifying cell attachment, proliferation, and metabolic activity—**A previously described DNA quantification assay was used to determine the number of cells attached to the scaffold [29]. Briefly, scaffolds were washed in PBS to remove unattached cells, placed in a papain solution to digest the scaffold and lyse the cells in order to expose their DNA, and then incubated with a Hoechst 33258 dye (Invitrogen, Carlsbad, CA) to fluorescently label double-stranded DNA [29,47]. Fluorescence intensities (352/461 nm excitation/emission) from each sample were read using a fluorescence spectrophotometer (Varian, Santa Clara, CA) and then compared to a standard curve created from known numbers of TCs. Cell numbers are reported as a percentage of the total number of seeded cells; numbers of attached cells at day 1 were considered to be a measure of initial cell attachment efficiency [22], while cell numbers at subsequent time points were considered a measure of cell proliferation.

Cell metabolic activity was determined using a previously described nondestructive alamarBlue assay [29,48]. Cell-seeded scaffolds were incubated at 37 °C in 1× alamarBlue (Invitrogen, Carlsbad, CA) solution with gentle shaking for 3 h. Resorufin fluorescence (570/585 nm excitation/emission) was read at using a fluorescence spectrophotometer (Varian, Santa Clara, CA) and compared to a standard curve created from known TCs of the same passage as those used in the experiment. Results are expressed as the total metabolic activity of the cells inside the scaffold relative to that of the initially seeded cells. Metabolic activity results were used as a proxy for relative cell health when the total number of attached cells was comparable [29].

**2.9. Statistical analysis—**One-way analysis of variance (ANOVA) was performed on membrane and mechanical data sets followed by Tukey-HSD post-hoc tests. Paired student *t*-tests were used to compare the two groups in cell viability experiments. Significance was set at $p < 0.05$. At least $n = 6$ scaffolds or membranes were used for all analyses. Error is reported in figures as standard deviation unless otherwise noted.

## 3. Results

### 3.1. CG membranes

CG membranes consistently displayed a dense network of fibrillar collagen content (Fig. 2(A)). The thickness of the final membrane was observed to increase with either the collagen-GAG wt% in the CG suspension or with the volume of suspension used (Fig. 2(B)). The experimental groups were created from either 0.5% w/v or 1% w/v CG suspensions with either 1× volume (25 mL) or 2× volume (50 mL) of suspension added to the Petri dish prior to drying in order to create four membrane variants: 23 ± 1, 35 ± 1 μm (0.5% w/v suspension; 1×, 2× volume); 45 ± 3 μm, 78 ± 3 μm (1% w/v suspension; 1×, 2× volume). Additionally, sequential ($n = 6$, 1% w/v suspension) addition of CG suspension to the same Petri dish during the process of evaporative drying was used to create membranes as thick as 240 μm.

All CG membranes were found to possess consistent relative densities between 0.75 and 0.80 (20–25% porous) (Fig. 2(B)). While statistically significant differences in membrane relative density were observed between some groups (1% w/v 1× vs. 0.5% w/v 2×, $p = 0.003$; 1% w/v 1× vs. 1% w/v 2×, $p = 0.009$), these differences do not suggest any trend. Swelling assays revealed that all four membrane variants tested (0.5% w/v 1×, 0.5% w/v 2×, 1% w/v 1×, and 1% w/v 2×) showed consistent hydration curves and were at least 90% hydrated after 30 min in PBS (data not shown).

### 3.2. Membrane mechanical properties

As expected due to random evaporative processes, the CG membranes were found to be isotropic in-plane. Dry specimens from 1% w/v 1× volume membranes were cut into samples from orthogonal directions ('parallel' vs. 'perpendicular' samples) and then pulled to failure. The tensile modulus of the *dry* membranes in the perpendicular orientation (636 ± 47 MPa) was not significantly different from the parallel orientation (693 ± 20 MPa) ($p$ = 0.06). Like with CG scaffolds, the tensile modulus of the CG membranes was found to increase significantly with crosslinking treatment and intensity [12]. The tensile moduli of *hydrated* CG membrane specimens (0.5% w/v 1×, 1% w/v 1×) was determined after no crosslinking (NC), dehydrothermal crosslinking (DHT), DHT plus carbodiimide crosslinking at a 1:1:5 EDAC:NHS:COOH molar ratio (EDAC 1:1:5), and DHT plus carbodiimide crosslinking at a 5:2:1 M ratio (EDAC 5:2:1). For the 0.5% w/v membranes, no significant difference was observed between the NC and DHT groups ($p$ = 0.86), but significant differences were observed between all other groups ($p \leq 0.01$, all groups). The tensile modulus of the hydrated 1% w/v 1× membranes was found to significantly increase with each increasing crosslinking step ($p \leq 0.02$, all groups), resulting in hydrated CG membranes showing tensile moduli approaching 30 MPa, multiple orders of magnitude stiffer than CG scaffolds (Fig. 3(A–B)). While there is a notable decrease in membrane modulus after hydration, this is consistent with previous results for CG scaffolds [12].

### 3.3. Aligned scaffold mechanical properties

All scaffolds displayed a consistent relative density (0.6%) [29]. The aligned CG scaffold variants (Pore sizes: 55 ± 18 μm, 243 ± 29 μm) displayed significantly higher *dry* tensile modulus (833 ± 236, 829 ± 165 kPa) compared to an isotropic CG control [45] ($p \leq 0.03$) (Fig. 3(C)). Cellular solids theory and previous experimental results predict that mechanical properties of a series of scaffolds with constant relative density and mean pore shape (*i.e.* degree of anisotropy) will be independent of pore size [9,12]. While slight differences in the aspect ratio (A.R., a measure of the degree of pore anisotropy) for the two aligned scaffolds have been previously reported (55 μm, 1.41 ± 0.16; 243 μm, 1.57 ± 0.23) [29], no difference in scaffold tensile modulus was observed between the anisotropic scaffolds ($p$ = 0.96).

### 3.4. Structural features of aligned scaffold-membrane core–shell composites

The CG scaffold core of the core–shell composites showed aligned, elongated pores in the longitudinal plane (Fig. 4(A)) and circular, more isotropic pores in the transverse plane (Fig. 4(B)) as a result of unidirectional heat transfer applied during freeze-drying. The CG membrane showed stable integration with the CG scaffold core (Fig. 4(C)), with limited delamination observed during freeze-drying, hydration, crosslinking, or mechanical testing processes.

### 3.5. Mechanical properties of aligned scaffold-membrane core–shell composites

Core-shell composites were created from a consistent aligned CG scaffold (pore size: 243 ± 29 μm) core and one of four 5:2:1 EDAC-crosslinked membranes of distinct thicknesses: 23 μm (0.5% w/v 1×), 45 μm (1% w/v 1×), 78 μm (1% w/v 2×), and 155 μm (1% w/v 2× wrapped twice around scaffold). A significant effect of membrane thickness was observed on the tensile modulus of the aligned scaffold-membrane core–shell composites ($p$ < 0.0001). While the increase in modulus between the core–shell composites with 23 μm and 45 μm thick membranes was not significant ($p$ = 0.14), significant differences were observed between all other groups ($p \leq 0.001$) (Fig. 5(A–B)). Scaffold-membrane composites also demonstrated dramatically increased tensile moduli over aligned CG scaffolds alone, with a 36-fold increase observed for the 155 μm membrane composite.

Experimental results closely mirrored theoretical predictions (solid line, Fig. 5(A)), indicating that the scaffold core and membrane shell were functionally integrated.

### 3.6. Tendon cell attachment and bioactivity in core–shell composite scaffolds

TC number and metabolic activity were assessed over a 14 day *in vitro* culture period within the aligned CG scaffolds alone (*No membrane*) or within the core–shell aligned scaffold-membrane composites (*Membrane*) (Fig. 6); both groups were fabricated with the identical scaffold microstructure (pore size: 243 μm). Early (1 day) results demonstrated that TC number was significantly increased in the core–shell composites ($p = 0.007$) (Fig. 6(A)). While both groups showed increases in TC number over time, no significant differences were observed between the groups at either day 7 ($p = 0.22$) or day 14 ($p = 0.33$). No significant difference was observed in TC metabolic activity at day 1 between the *Membrane* and *No membrane* groups ($p > 0.05$) (Fig. 6(B)). While TC metabolic activity in the scaffold alone was significantly higher than that in the core–shell composite at day 7 ($p = 0.01$), TC metabolic activity in the core–shell composites was elevated compared to day 1 and there were no significant differences in metabolic activity between groups at day 14 ($p > 0.05$).

## 4. Discussion

This paper describes the development of a CG scaffold-membrane (core–shell) composite for tendon tissue engineering with the intent to avoid aspects of the typical tradeoff between mechanical properties (i.e. modulus, failure strength) and bioactivity (permeability and porosity) for porous tissue engineering scaffolds. Cellular solids modeling provides the framework to describe the tradeoff between mechanical properties and bioactivity proxies (specific surface area, permeability, steric hindrance) as a function of scaffold relative density [9,12,13,22,23,29]. Namely, with increasing scaffold $\rho^*/\rho_s$, modulus ($E \sim (\rho^*/\rho_s)^2$) and specific surface area ($SA/V \sim (\rho^*/\rho_s)^{0.5}$) increase, but permeability decreases ($k \sim (1–\rho^*/\rho_s)^{1.5}$) and steric hindrance to cell penetration increases. These relations also predict that to increase CG scaffold elastic modulus by the ~2 orders of magnitude necessary to achieve levels suitable to prevent mechanical failure in the case of *in vivo* tendon applications, the scaffold relative density would have to be increased from 0.006 to 0.05–0.15. While there are techniques to create CG scaffolds with solid content approaching these levels [20], an increase of this magnitude would result in sharp declines in both porosity, permeability, and the ability of cells to penetrate into the scaffold microstructure. The resultant decrease in bioactivity would likely make the scaffolds unsuitable for tendon tissue engineering. Taking inspiration from mechanically efficient core–shell structures in nature [10], we felt the scaffold-membrane composite paradigm may provide an alternative strategy to overcome these limitations.

We describe an evaporative process to fabricate CG membranes with tailorable thicknesses over an order of magnitude (23–240 μm), but consistent relative densities of ~0.75–0.80 that are significantly higher than those of the CG scaffold (0.006) (Fig. 2(B)). CG membranes were mechanically isotropic in-plane, and as with CG scaffolds [12,19] increasing the degree of physical (DHT) or chemical (carbodiimide) crosslinking significantly increased membrane tensile moduli (Fig. 2(A–B)). The EDAC 5:2:1 groups displayed ~7–10 fold increases in modulus over non-crosslinked controls, comparable in magnitude shift to previous work with CG scaffolds [12]. Additionally, CG membranes were observed to swell with similar kinetics as previously observed for CG scaffolds [20] and to reach an asymptote, suggesting a stable membrane structure.

We have previously described a directional solidification approach to fabricate CG scaffolds with defined levels of anisotropy [29] where TC attachment, proliferation, metabolic

activity, and degree of TC populational alignment were all shown to be critically affected by both scaffold pore size and degree of anisotropy [29]. Here we investigated the effect of scaffold anisotropy on its tensile properties and the capacity of the core–shell paradigm to significantly improve construct properties. Aligned tissue engineering scaffolds have consistently demonstrated superior mechanical properties along the axis of alignment compared to isotropic controls [5,49], though these results have mainly been shown using 2D electrospun materials or single unit cell thick honeycomb-like structures [50]. We showed that two aligned CG scaffold variants with significantly different pore sizes (55, 243 μm) had tensile moduli nearly three times greater than that of an isotropic CG scaffold control fabricated at the same relative density (Fig. 3(C)). For a series of scaffolds with constant $\rho^*/\rho_s$ such as the three scaffolds tested here, cellular solids theory and previous results [9,12] allowed us to make two predictions regarding scaffold mechanical properties. First, that scaffold modulus is a function of relative density but not pore diameter. This was confirmed by showing that aligned scaffolds with identical relative densities but different pore sizes had nearly identical tensile moduli (Fig. 3(C)). Second, that scaffold modulus should increase with pore anisotropy (when scaffolds are tested in the direction of anisotropy); this was confirmed by showing the significant increase in anisotropic scaffold modulus relative to the isotropic control (Fig. 3(C)). We then applied cellular solids theory to predict changes in the elastic moduli of anisotropic vs. isotropic open cell foams. Here, the predicted modulus of the anisotropic scaffolds ($E_a^*$) can be described with the isotropic scaffold modulus ($E_i^*$) and the anisotropic:isotropic scaffold pore aspect ratios ($R$):

$$E_a^* = E_i^* \left( \frac{2R^2}{1+(1/R)^3} \right) \quad (2)$$

Based on the previously reported aspect ratios of the 55 μm and 243 μm aligned scaffolds neglecting the end sections held in the clamps during tensile testing [29] the predicted moduli would be 880 kPa and 913 kPa for the 55 μm and 243 μm scaffolds, comparing favorably to the experimentally achieved values of 833 ± 236 kPa and 829 ± 165 kPa.

We fabricated CG scaffold-membrane core–shell composites via liquid–solid phase co-synthesis [37] in a manner aimed at achieving functional integration between CG scaffold and membrane components by allowing a hydration time-step for the CG suspension to hydrate the membrane prior to freezing. SEM confirmed the creation of an aligned microstructure in the longitudinal plane (Fig. 4(A)) while the transverse plane showed a more isotropic structure (Fig. 4(B)), consistent with results previously reported for the aligned CG scaffold alone [29]. These results indicate that addition of the CG membrane did not adversely influence the directional solidification process required to create the aligned CG scaffold microstructure, and was expected because the CG membrane should not alter the degree of thermal conductivity mismatch ($k_{Cu}/k_{PTFE} \sim 1600$) in the composite mold [29]. Importantly, it was demonstrated that the CG membrane could be integrated into the CG scaffold structure to form a continuous composite material (Fig. 4(C)) that exhibited limited delamination during fabrication, structural and mechanical analysis, and *in vitro* cell culture components of this study. Comparatively, wrapping the membrane around a complete scaffold required gluing or sutures to prevent delamination. The degree of membrane incorporation theoretically could be tuned by adjusting the hydration time of the membrane in the scaffold suspension prior to freeze-drying, presenting a future avenue for testing and development, particularly in the light of the mechanical results discussed below.

After separately characterizing the mechanical properties of the aligned CG scaffolds and CG membranes, CG scaffold-membrane composites were fabricated and characterized using membranes ranging in thicknesses from 23 μm (0.5% w/v 1×) to 155 μm (1% w/v 2×

wrapped twice around scaffold). These composites demonstrated dramatically increased tensile moduli over CG scaffold controls (no membrane shell) with a 36-fold increase observed for the 155 μm thick membrane (Fig. 5). The aspect ratios of the scaffold, membrane, and scaffold-membrane samples tested in tension were consistent within groups. However, because the membrane sample aspect ratios were greater than the scaffold and scaffold-membrane samples, it is possible that the extension behavior of the membrane vs. scaffolds was different due to differential stress propagation in the specimens. While minimal impact is expected and all in-group comparisons are consistent, future work will examine creep dependent behavior of these composites.

Experimental results for the scaffold-membrane composite were also compared to predictions from layered composites theory, which has previously been used to accurately predict the tensile properties of multicomponent materials based on the relative size of the individual components and their separate moduli [38]. Experimental results correlated well with theoretical predictions, especially for composites with the two thicker membranes (78 μm, 155 μm). However, the experimental values for tensile moduli of the core–shell composites with the two thinnest membranes (23, 45 μm) fell somewhat short of theoretical predictions from layered composite theory (Fig. 5(A)). These results may suggest a degree of incomplete integration between the core and shell components for the thinnest shell composites, with superior, more complete incorporation observed for the thicker membranes with the scaffold core. However the composites with the thinnest shells were fabricated only to test a wider range of composite structures and are not anticipated to be used for *in vivo* tendon tissue engineering applications. Overall, the close agreement of the experimental results with the theoretical predictions as well as the low incidence of composite delamination suggests that the core–shell scaffolds behave like layered composites, implying adequate integration of the membrane with the scaffold.

While the scaffold core maintains an open-pore structure conducive for cell penetration and efficient metabolite transport, addition of the CG membrane shell covering ~75% of the scaffold surface requires assessing cell proliferation and metabolic activity within the composite structure in order to determine its effect on nutrient and oxygen transport into the construct. Typical diffusion distances in CG scaffolds are on the order of 1–2 mm [51], implying the scaffold geometry used here will at minimum provide an environment at its core with reduced metabolite transport. Based on previous results showing that collagen membranes are typically cell-impermeable but that depending on membrane density can be metabolite and small biomolecule permeable [52], we hypothesized that addition of a 20–25% porous CG membrane shell would not significantly reduce the bioactivity of TCs seeded within the scaffold due to adequate maintenance of metabolite transport. TC number and metabolic activity were measured over a 14 day *in vitro* culture period in aligned CG scaffold cores (pore size: 243 ± 29 μm) with (*Membrane*) and without (*No membrane*) CG membrane shells. After 1 day in culture, the total number of attached TCs was observed to significantly ($p = 0.007$) increase in CG membrane scaffolds relative to the scaffold alone (Fig. 6(A)), with no significant difference ($p = 0.22$) in the metabolic activity (Fig. 6(B)). This result is likely a consequence of the cell-impermeable membrane impacting cell-loss during the seeding step; it is likely that the membrane prevented the cell suspension seeded onto the scaffold from leaking out of the sides, thereby improving cell attachment relative to the scaffold alone where additional cells might be lost. Later time points, a measure of TC proliferation, showed dramatic increases in cell number and metabolic activity compared to day 1 for both groups (Fig. 6(A)). TC number and metabolic activity increased for both groups from day 1 to day 7 and showed further increases at day 14, with no significant differences observed between the groups at this final time point (Fig. 6(A–B)). These results indicate that the core–shell constructs have adequate permeability to support the nutrient and metabolite transport necessary for sustained TC viability and proliferation. We also

recognize the need for additional metrics beyond viability data to more fully characterize the behavior of TCs in these composites. Ongoing work in our lab is using real-time PCR to quantify the expression of tendon-related markers as a function of scaffold microstructural, mechanical, and chemical properties.

The membrane design presented here has adequate permeability to maintain long-term cell viability *in vitro*, but it is cell-impermeable. While adequate TC proliferation and metabolic activity was observed, this was for the case where cells were seeded onto either end of the construct for *in vitro* assays. For acellular *in vivo* deployment into a tendon defect, it may be necessary to facilitate cell penetration from all directions. To that end, we are currently developing a periodically perforated CG membrane that contains large (250–500 μm) openings to facilitate radial cell penetration and assessing cell bioactivity in larger scaffold-membrane composites. To further improve composite mechanical competence, we are also developing a new series of anisotropic CG scaffolds with moderately increased relative density (0.012, 0.018) compared to the current constructs (0.006). Cellular solids theory predicts that these materials will show a 4–9-fold increase in tensile modulus with minimal reductions in porosity and permeability. These materials are also well suited for integration with recently developed techniques in our lab that enable photolithography-based sequestration of biomolecules within the scaffolds [53] in order to further improve scaffold bioactivity.

## 5. Conclusions

This paper describes development of a core–shell CG biomaterial composite that successfully integrates a high density outer shell (isotropic CG membrane) with a low density porous core (anisotropic CG scaffold). The membrane thickness can be controlled over a wide range (23–240 μm) and the composite Young's modulus can be predicted by layered composites theory. The addition of a membrane shell significantly increases the core–shell composite tensile modulus in a manner consistent with layered composite theory. This paradigm allows us to circumvent a conventional limitation in biomaterial scaffolds design where construct mechanical strength and porosity are inversely related. Further, these composites also demonstrate the capability to support TC attachment, proliferation, and viability out to 14 days at comparable levels to CG scaffolds alone, indicating CG membranes possess adequate permeability to support cell bioactivity within the scaffold structure. Future work will continue to optimize membrane design and integration while progressing toward *in vivo* preclinical and clinical applications.

## Acknowledgments

The authors would like to acknowledge Dr. Hyunjoon Kong for the use of his mechanical tester, Dr. Jim Mabon (MRL, UIUC) for his assistance with SEM analysis, and Dr. Charles Schroeder (ChBE, UIUC) for the use of his fluorescence spectrophotometer. We are grateful for the funding for this study provided by the Chemistry–Biology Interface Training Program NIH NIGMS T32GM070421 (SRC), the Chemical and Biomolecular Engineering Dept. (SRC, BAH), and the Institute for Genomic Biology (SRC, BAH) at the University of Illinois at Urbana-Champaign. This research was carried out in part in the Frederick Seitz Materials Research Laboratory Central Facilities, University of Illinois, which are partially supported by the U.S. Department of Energy under grants DE-FG02-07ER46453 and DE-FG02-07ER46471.

## References

[1]. James R, Kesturu G, Balian G, Chhabra AB. Tendon: biology, biomechanics, repair, growth factors, and evolving treatment options. J Hand Surg-Am. 2008; 33A:102–12. [PubMed: 18261674]

[2]. Liu Y, Ramanath HS, Wang DA. Tendon tissue engineering using scaffold enhancing strategies. Trends Biotechnol. 2008; 26:201–9. [PubMed: 18295915]

[3]. Butler DL, Juncosa-Melvin N, Boivin GP, Galloway MT, Shearn JT, Gooch C, et al. Functional tissue engineering for tendon repair: a multidisciplinary strategy using mesenchymal stem cells, bioscaffolds, and mechanical stimulation. J Orthop Res. 2008; 26:1–9. [PubMed: 17676628]

[4]. Li X, Xie J, Lipner J, Yuan X, Thomopoulos S, Xia Y. Nanofiber scaffolds with gradations in mineral content for mimicking the tendon-to-bone insertion site. Nano Lett. 2009; 9:2763–8. [PubMed: 19537737]

[5]. Moffat KL, Kwei AS, Spalazzi JP, Doty SB, Levine WN, Lu HH. Novel nanofiber-based scaffold for rotator cuff repair and augmentation. Tissue Eng Part A. 2009; 15:115–26. [PubMed: 18788982]

[6]. Pham QP, Sharma U, Mikos AG. Electrospinning of polymeric nanofibers for tissue engineering applications: a review. Tissue Eng. 2006; 12:1197–211. [PubMed: 16771634]

[7]. Sahoo S, Toh SL, Goh JC. A bFGF-releasing silk/PLGA-based biohybrid scaffold for ligament/tendon tissue engineering using mesenchymal progenitor cells. Biomaterials. 2010; 31:2990–8. [PubMed: 20089300]

[8]. Altman GH, Horan RL, Lu HH, Moreau J, Martin I, Richmond JC, et al. Silk matrix for tissue engineered anterior cruciate ligaments. Biomaterials. 2002; 23:4131–41. [PubMed: 12182315]

[9]. Gibson, LJ.; Ashby, MF.; Harley, BA. Cellular materials in nature and medicine. Cambridge University Press; Cambridge, U.K: 2010.

[10]. Gibson LJ. Biomechanics of cellular solids. J Biomech. 2005; 38:377–99. [PubMed: 15652536]

[11]. Harley BAC, Gibson LJ. In vivo and in vitro applications of collagen-GAG scaffolds. Chem Eng J. 2008; 137:102–21.

[12]. Harley BA, Leung JH, Silva EC, Gibson LJ. Mechanical characterization of collagen-glycosaminoglycan scaffolds. Acta Biomater. 2007; 3:463–74. [PubMed: 17349829]

[13]. O'Brien FJ, Harley BA, Waller MA, Yannas IV, Gibson LJ, Prendergast PJ. The effect of pore size on permeability and cell attachment in collagen scaffolds for tissue engineering. Technol Health Care. 2007; 15:3–17. [PubMed: 17264409]

[14]. Yannas IV, Tzeranis DS, Harley BA, So PT. Biologically active collagen-based scaffolds: advances in processing and characterization. Philos T R Soc A. 2010; 368:2123–39.

[15]. Juncosa-Melvin N, Shearn JT, Boivin GP, Gooch C, Galloway MT, West JR, et al. Effects of mechanical stimulation on the biomechanics and histology of stem cell-collagen sponge constructs for rabbit patellar tendon repair. Tissue Eng. 2006; 12:2291–300. [PubMed: 16968169]

[16]. Saber S, Zhang AY, Ki SH, Lindsey DP, Smith RL, Riboh J, et al. Flexor tendon tissue engineering: bioreactor cyclic strain increases construct strength. Tissue Eng Part A. 2010; 16:2085–90. [PubMed: 20109062]

[17]. Chokalingam K, Juncosa-Melvin N, Hunter SA, Gooch C, Frede C, Florert J, et al. Tensile stimulation of murine stem cell-collagen sponge constructs increases collagen type I gene expression and linear stiffness. Tissue Eng Part A. 2009; 15:2561–70. [PubMed: 19191514]

[18]. Kuo CK, Tuan RS. Mechanoactive tenogenic differentiation of human mesenchymal stem cells. Tissue Eng Part A. 2008; 14:1615–27. [PubMed: 18759661]

[19]. Yannas IV, Lee E, Orgill DP, Skrabut EM, Murphy GF. Synthesis and characterization of a model extracellular matrix that induces partial regeneration of adult mammalian skin. Proc Natl Acad Sci USA. 1989; 86:933–7. [PubMed: 2915988]

[20]. Harley BA, Spilker MH, Wu JW, Asano K, Hsu HP, Spector M, et al. Optimal degradation rate for collagen chambers used for regeneration of peripheral nerves over long gaps. Cells Tissues Organs. 2004; 176:153–65. [PubMed: 14745243]

[21]. Yannas, IV. Tissue and organ regeneration in adults. Springer; New York: 2001.

[22]. O'Brien FJ, Harley BA, Yannas IV, Gibson LJ. The effect of pore size on cell adhesion in collagen-GAG scaffolds. Biomaterials. 2005; 26:433–41. [PubMed: 15275817]

[23]. Harley BAC, Kim HD, Zaman MH, Yannas IV, Lauffenburger DA, Gibson LJ. Microarchitecture of three-dimensional scaffolds influences cell migration behavior via junction interactions. Biophys J. 2008; 95:4013–24. [PubMed: 18621811]

[24]. Farrell E, O'Brien FJ, Doyle P, Fischer J, Yannas I, Harley BA, et al. A collagen-glycosaminoglycan scaffold supports adult rat mesenchymal stem cell differentiation along osteogenic and chondrogenic routes. Tissue Eng. 2006; 12:459–68. [PubMed: 16579679]

[25]. Torres DS, Freyman TM, Yannas IV, Spector M. Tendon cell contraction of collagen-GAG matrices in vitro: effect of cross-linking. Biomaterials. 2000; 21:1607–19. [PubMed: 10885733]

[26]. Harley BA, Freyman TM, Wong MQ, Gibson LJ. A new technique for calculating individual dermal fibroblast contractile forces generated within collagen-GAG scaffolds. Biophys J. 2007; 93:2911–22. [PubMed: 17586570]

[27]. O'Brien FJ, Harley BA, Yannas IV, Gibson L. Influence of freezing rate on pore structure in freeze-dried collagen-GAG scaffolds. Biomaterials. 2004; 25:1077–86. [PubMed: 14615173]

[28]. Haugh MG, Murphy CM, O'Brien FJ. Novel freeze-drying methods to produce a range of collagen-glycosaminoglycan scaffolds with tailored mean pore sizes. Tissue Eng Part C Methods. 2010; 16:887–94. [PubMed: 19903089]

[29]. Caliari SR, Harley BAC. The effect of anisotropic collagen-GAG scaffolds and growth factor supplementation on tendon cell recruitment, alignment, and metabolic activity. Biomaterials. 2011; 32:5330–40. [PubMed: 21550653]

[30]. Dressler MR, Butler DL, Boivin GP. Age-related changes in the biomechanics of healing patellar tendon. J Biomech. 2006; 39:2205–12. [PubMed: 16120443]

[31]. Shearn JT, Juncosa-Melvin N, Boivin GP, Galloway MT, Goodwin W, Gooch C, et al. Mechanical stimulation of tendon tissue engineered constructs: effects on construct stiffness, repair biomechanics, and their correlation. J Biomech Eng. 2007; 129:848–54. [PubMed: 18067388]

[32]. Guo R, Xu S, Ma L, Huang A, Gao C. The healing of full-thickness burns treated by using plasmid DNA encoding VEGF-165 activated collagen-chitosan dermal equivalents. Biomaterials. 2011; 32:1019–31. [PubMed: 21071076]

[33]. Amado S, Rodrigues JM, Luis AL, Armada-da-Silva PA, Vieira M, Gartner A, et al. Effects of collagen membranes enriched with in vitro-differentiated N1E-115 cells on rat sciatic nerve regeneration after end-to-end repair. J Neuroeng Rehabil. 2010; 7:7. [PubMed: 20149260]

[34]. Lee CK, Koo KT, Kim TI, Seol YJ, Lee YM, Rhyu IC, et al. Biological effects of a porcine-derived collagen membrane on intrabony defects. J Periodontal Implant Sci. 2010; 40:232–8. [PubMed: 21072220]

[35]. Utsunomiya H, Koh H, Miyamoto J, Sakai T. High-strength porous copper by cold-extrusion. Adv Eng Mater. 2008; 10:826–9.

[36]. Nerurkar NL, Sen S, Huang AH, Elliott DM, Mauck RL. Engineered disc-like angle-ply structures for intervertebral disc replacement. Spine. 2010; 35:867–73. [PubMed: 20354467]

[37]. Harley BA, Lynn AK, Wissner-Gross Z, Bonfield W, Yannas IV, Gibson LJ. Design of a multiphase osteochondral scaffold III: fabrication of layered scaffolds with continuous interfaces. J Biomed Mater Res A. 2010; 92:1078–93. [PubMed: 19301263]

[38]. Allen, HG. Analysis and design of structural sandwich panels. 1st ed. Pergamon Press; New York: 1969.

[39]. Pins GD, Toner M, Morgan JR. Microfabrication of an analog of the basal lamina: biocompatible membranes with complex topographies. Faseb J. 2000; 14:593–602. [PubMed: 10698975]

[40]. Olde Damink LH, Dijkstra PJ, van Luyn MJ, van Wachem PB, Nieuwenhuis P, Feijen J. Cross-linking of dermal sheep collagen using a water-soluble carbodiimide. Biomaterials. 1996; 17:765–73. [PubMed: 8730960]

[41]. Yannas IV, Tobolsky AV. Cross-linking of gelatine by dehydration. Nature. 1967; 215:509–10. [PubMed: 6057911]

[42]. Yannas IV, Burke JF, Gordon PL, Huang C, Rubenstein RH. Design of an artificial skin. II. Control of chemical composition. J Biomed Mater Res. 1980; 14:107–32. [PubMed: 7358747]

[43]. Vickers SM, Squitieri LS, Spector M. Effects of cross-linking type II collagen-GAG scaffolds on chondrogenesis in vitro: dynamic pore reduction promotes cartilage formation. Tissue Eng. 2006; 12:1345–55. [PubMed: 16771647]

[44]. Freyman TM, Yannas IV, Yokoo R, Gibson LJ. Fibroblast contraction of a collagen-GAG matrix. Biomaterials. 2001; 22:2883–91. [PubMed: 11561894]

[45]. Kanungo BP, Gibson LJ. Density-property relationships in collagen-glycosaminoglycan scaffolds. Acta Biomater. 2010; 6:344–53. [PubMed: 19770077]

[46]. Kapoor A, Caporali EH, Kenis PJ, Stewart MC. Microtopographically patterned surfaces promote the alignment of tenocytes and extracellular collagen. Acta Biomater. 2010; 6:2580–9. [PubMed: 20045087]

[47]. Kim YJ, Sah RL, Doong JY, Grodzinsky AJ. Fluorometric assay of DNA in cartilage explants using Hoechst 33258. Anal Biochem. 1988; 174:168–76. [PubMed: 2464289]

[48]. Tierney CM, Jaasma MJ, O'Brien FJ. Osteoblast activity on collagen-GAG scaffolds is affected by collagen and GAG concentrations. J Biomed Mater Res A. 2009; 91:92–101. [PubMed: 18767061]

[49]. Shang S, Yang F, Cheng X, Walboomers XF, Jansen JA. The effect of electrospun fibre alignment on the behaviour of rat periodontal ligament cells. Eur Cells Mater. 2010; 19:180–92.

[50]. Engelmayr GC Jr, Cheng M, Bettinger CJ, Borenstein JT, Langer R, Freed LE. Accordion-like honeycombs for tissue engineering of cardiac anisotropy. Nat Mater. 2008; 7:1003–10. [PubMed: 18978786]

[51]. Harley, BA.; Yannas, IV. In vivo synthesis of tissues and organs. In: Lanza, R.; Langer, R.; Vacanti, JP., editors. Principles of tissue engineering. 3rd ed. Elsevier/Academic Press; 2007.

[52]. Kimura Y, Hokugo A, Takamoto T, Tabata Y, Kurosawa H. Regeneration of anterior cruciate ligament by biodegradable scaffold combined with local controlled release of basic fibroblast growth factor and collagen wrapping. Tissue Eng Part C Methods. 2008; 14:47–57. [PubMed: 18454645]

[53]. Martin TA, Caliari SR, Williford PD, Harley BA, Bailey RC. The generation of biomolecular patterns in highly porous collagen-GAG scaffolds using direct photolithography. Biomaterials. 2011; 32:3949–57. [PubMed: 21397322]

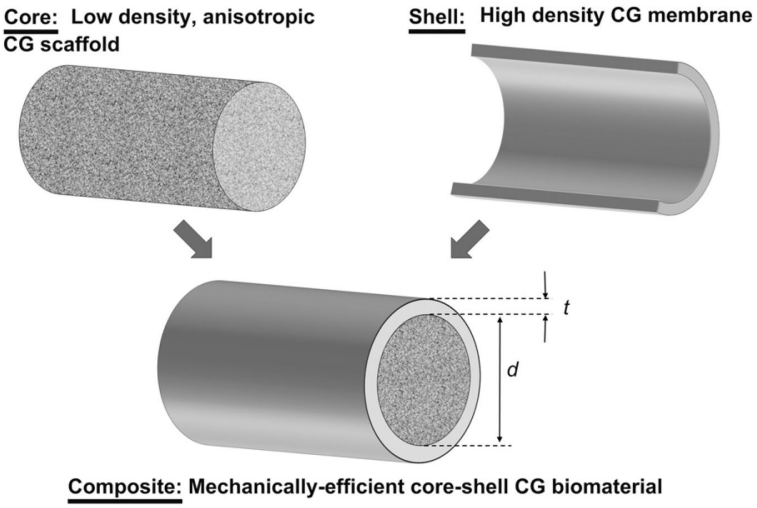


**Fig. 1.**
Schematic of CG scaffold-membrane composite design.

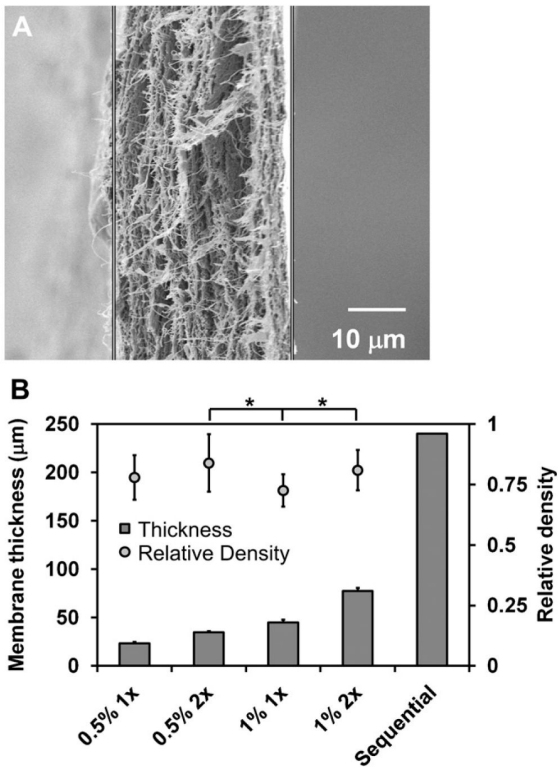


**Fig. 2.**

A) Cross-sectional SEM image of the CG membrane illustrating the dense, layered fibrillar organization. Scale bar: 10 μm. B) CG membranes can be produced over a wide range of thicknesses (23–240 μm) with consistent relative density (0.75–0.80) (*n* = 17). Error bars: Mean ± SD.

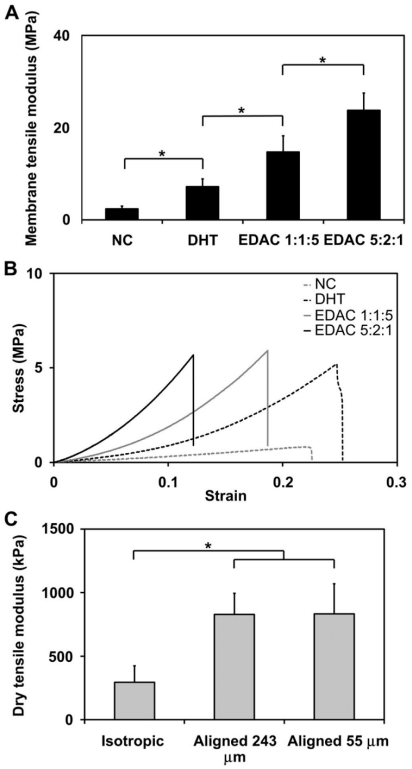


**Fig. 3.**

A) Effect of increasing the intensity of crosslinking on the tensile modulus of 1% w/v 1× CG membranes ($n = 6$). B) Comparison of stress-strain curves for each 1% w/v 1× CG membrane variant. Increasing crosslinking treatments: NC (non-crosslinked), DHT (dehydrothermal crosslinked), EDAC 1:1:5 and EDAC 5:2:1 (EDAC:NHS:COOH ratios). C) Both aligned CG scaffolds have significantly higher tensile moduli than isotropic CG controls (adapted from [1]; $n = 6$). No significant difference was observed in tensile modulus between aligned CG scaffolds fabricated at two different pore sizes (243 μm, 55 μm). Error bars: Mean ± SD.

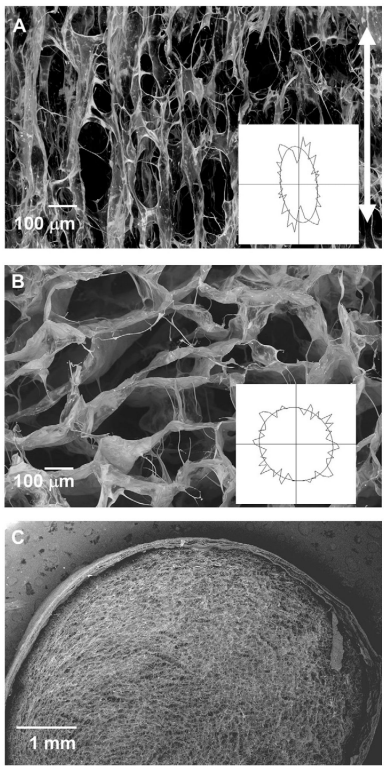


**Fig. 4.**

A) SEM image of a representative longitudinal CG scaffold section shows the aligned, elongated pore structure present in the anisotropic cores of the core–shell scaffolds. The vertical white arrow indicates the direction of heat transfer during directional solidification. Scale bar: 100 μm. B) SEM image of a representative transverse section through the scaffold displays the round, isotropic pore structure. Scale bar: 100 μm. C) SEM image of transverse plane of the scaffold-membrane composite showing the integration of the two regions. Scale bar: 1 mm.

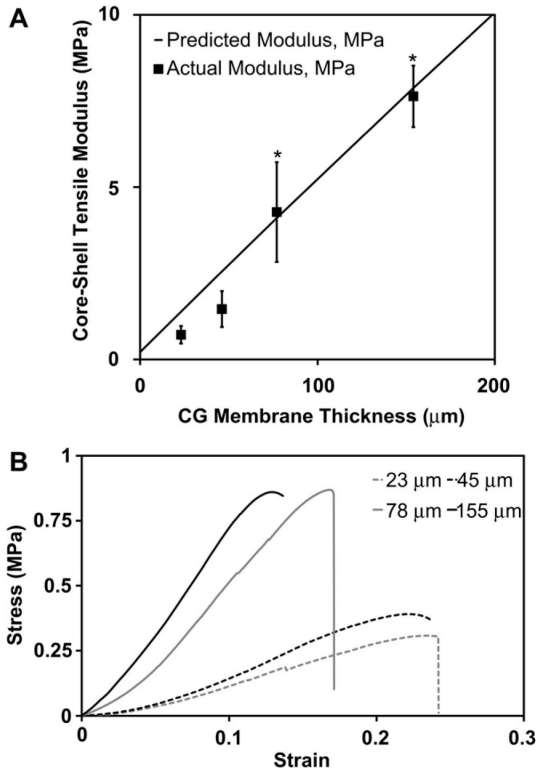


**Fig. 5.**

A) The tensile modulus of the core–shell CG composites increases significantly with membrane thickness. The experimentally measure tensile modulus ($n$ = 6, black squares) compares favorably to the predicted composite modulus obtained from layered composites theory (black line). The close agreement is indicative of integration of the membrane shell with scaffold core. Error bars: Mean ± SD. B) Representative stress-strain curves for the series of core–shell composites with increasing shell thickness.

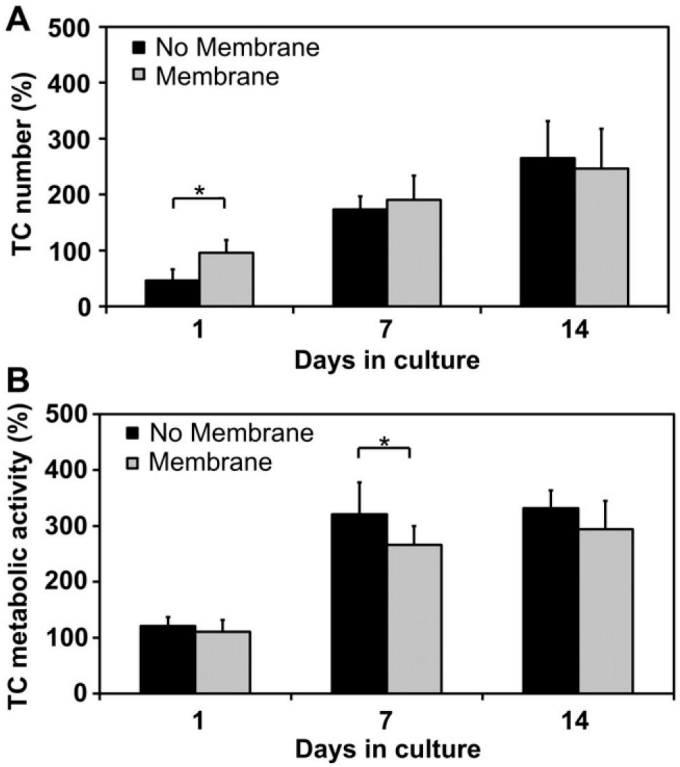


**Fig. 6.**

A) Core-shell CG composites (*Membrane*) support significantly higher TC number at day 1 ($n = 6$) and similar cell number at days 7 and 14 ($n = 6$) compared to CG scaffolds alone (*No membrane*). Both groups show large increases in TC number from day 1 to day 7 and day 7 to day 14. B) CG scaffolds alone (*No membrane*) display higher TC metabolic activity at day 1 ($n = 18$), significantly higher metabolic activity at day 7 ($n = 12$), and higher TC metabolic activity at day 14 ($n = 6$) compared to the core–shell CG composites (*Membrane*). However, both groups show large increases in TC metabolic activity from day 1 to day 7 and subsequent maintenance of metabolic activity through day 14. Error bars: Mean ± SD.